Icarus **156**, 485–497 (2002)
doi:10.1006/icar.2001.6804, available online at http://www.idealibrary.com on IDEAL®

Temporal Behavior of Stratospheric Ammonia Abundance and Temperature Following the SL9 Impacts

Kelly Fast,[1] Theodor Kostiuk, Paul Romani, and Fred Espenak

Planetary Systems Branch, Laboratory for Extraterrestrial Physics, NASA Goddard Space Flight Center, Greenbelt, Maryland 20771
E-mail: Kelly.Fast@gsfc.nasa.gov

Tilak Hewagama[2]

Department of Astronomy, University of Maryland, College Park, Maryland 20742-2421

Albert Betz and Rita Boreiko

CASA, University of Colorado, 593 UCB, Boulder, Colorado 80303

and

Timothy Livengood[2]

Challenger Center for Space Science Education, 1029 North Royal Street, Suite 300, Alexandria, Virginia 22314

Received March 13, 2001; revised September 4, 2001

Infrared emission lines of stratospheric ammonia (NH_3) were observed following the collisions of the fragments of Comet Shoemaker–Levy 9 with Jupiter in July of 1994 at the impact sites of fragments G and K. Infrared heterodyne spectra near 10.7 μm were obtained by A. Betz *et al.* (in *Abstracts for Special Sessions on Comet Shoemaker-Levy 9, The 26th Meeting of the Division for Planetary Sciences, Washington DC, 31 Oct.–4 Nov. 1994*, p. 25) using one of the Infrared Spatial Interferometer telescope systems on Mount Wilson. Lineshapes of up to three different NH_3 emission lines were measured at a resolving power of $\sim 10^7$ at multiple times following the impacts. We present here our radiative transfer analysis of the fully resolved spectral lineshapes of the multiple rovibrational lines. This analysis provides information on temperature structure and NH_3 abundance distributions and their temporal changes up to 18 days after impact. These results are compared to photochemical models to determine the role of photochemistry and other mechanisms in the destruction and dilution of NH_3 in the jovian stratosphere after the SL9 impacts.

One day following the G impact, the inferred temperature above 0.001 mbar altitude is 283 ± 13 K, consistent with a recent plume splashback model. Cooling of the upper stratosphere to 204 K by the fourth day and to quiescence after a week is consistent with a simple gray atmosphere radiative flux calculation and mixing with cold jovian air. During the first 4 days after impact, NH_3 was present primarily at altitudes above 1 mbar with a column density of $(7.7 \pm 1.6) \times 10^{17}$ cm^{-2} after 1 day and $(3.7 \pm 0.8) \times 10^{17}$ cm^{-2} after 4 days. (Errors represent precision.) We obtained >2.5 times more NH_3 than can be supplied by nitrogen from a large cometary fragment, suggesting a primarily jovian source for the NH_3. By 18 days postimpact, a return to quiescent upper stratospheric temperature is retrieved for the G region, with an NH_3 column density of 7.3×10^{17} cm^{-2} or more in the lower stratosphere, possibly supplied by NH_3 upwelling across an impact-heated and turbulent tropopause, which may have been masked by initial dust and haze. Above the 1-mbar level, the maximum retrieved column density decreased to 6.5×10^{16} cm^{-2}. Comparison to photochemical models indicates that photolysis alone is not sufficient to account for the loss of NH_3 above 1 mbar by that time, even when chemical reformation of NH_3 is ignored. We speculate that the dispersion of plume material at high altitudes (above 1 mbar) is responsible for the change in the spectra observed a few days postimpact. Data on the K impact region provide qualitatively consistent results.

Key Words: **Comets S-L9; Jupiter; Jupiter—atmosphere; infrared observations; photochemistry.**

INTRODUCTION

The collision of comet Shoemaker–Levy 9 with Jupiter in July of 1994 provided a unique opportunity to investigate not only planetary impacts but also jovian composition, photochemistry, and thermal rebound. Knowledge of the time scales for

[1] Formerly at Department of Astronomy, University of Maryland, College Park, MD 20742-2421.

[2] Also at Planetary Systems Branch, Laboratory for Extraterrestrial Physics, NASA Goddard Space Flight Center, Greenbelt, MD 20771.

0019-1035/02 $35.00

TABLE I
Molecular Line Parameters

NH_3 transition	Frequency (cm^{-1})	Lower state energy (cm^{-1})	Intensity[a] (cm^{-2} atm^{-1})
aQ(2,2)	931.3332	45.6	5.43
aQ(6,6)	927.3229	284.4	11.18
aQ(9,8)	926.0457	656.4	1.08

Source. HITRAN, Rothman *et al*. 1992.
[a] Intensities at 296 K, later scaled to model temperature.

the cooling of the atmosphere back to a quiescent state and the destruction of deposited species not normally found in the stratosphere would help to better understand the impacts themselves and provide a test for jovian photochemical models. Ammonia (NH_3), which was injected into the stratosphere by the SL9 impacts, is an effective probe of its photochemistry as well as the stratospheric thermal structure following the collisions. Here we report results of retrievals from a unique set of measurements taken up to 18 days after impact, at a spectral resolution that can fully resolve the shapes of narrow stratospheric NH_3 emission lines.

Infrared heterodyne spectroscopy with a resolving power of $\sim 10^7$ permits measurement of the true line profiles, revealing information about the temperature, abundance, and altitude distribution of the source species in the region of line formation. The portion of the data set acquired by Betz *et al*. (1994) that is examined in this paper provides important temporal information. The spectra were acquired on three occasions over an 18-day period following the impacts in the G region (Fig. 1). Multiple observations of the K region were also made (Fig. 2), following the nearby smaller impact of fragment W. The current measurements include emission profiles of several NH_3 transitions, each of different line intensity and lower state energy (Table I).

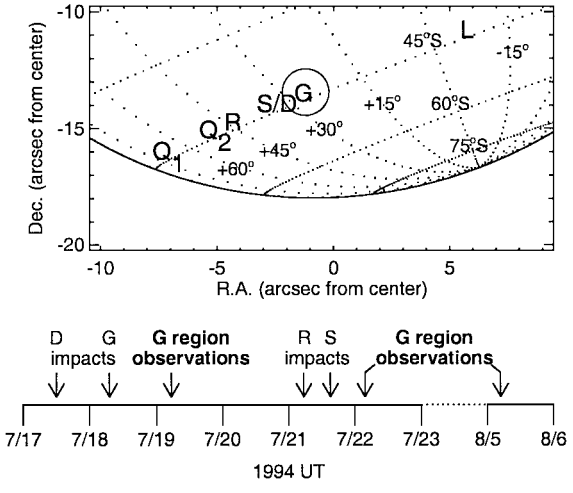

FIG. 1. Jupiter aspect geometry showing impact latitude and the instrumental field-of-view of 2 arcsec. The timeline shows the G region observation times relative to the different impact times.

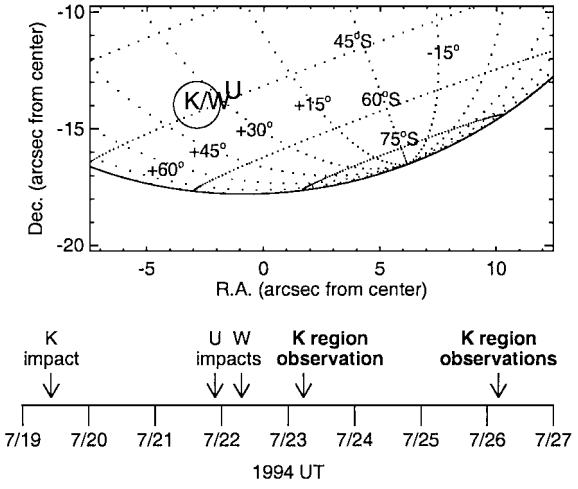

FIG. 2. K region observation timeline. All K region observations were made after the impacts that affected that region had ceased.

The different line intensities and the different dependence of each line emission on temperature provided a significant constraint on the temperature and the altitude distribution of NH_3 abundance in the emitting region. This is an improvement over a similar analysis of infrared heterodyne spectra from impacts Q1 and R (Kostiuk *et al*. 1996) that retrieved information on NH_3 altitude distribution and abundance based on a single line measured about a week after each impact.

We used a beam-integrated radiative transfer analysis developed by Goldstein (1989) and Hewagama *et al*. (in preparation), and retrieved temporal changes in NH_3 abundance and stratospheric temperature and their altitude distributions on Jupiter. We test new photochemical models, which include photochemical destruction and recycling of NH_3 due to the effects of a changing atmospheric temperature over the observing period.

OBSERVATIONS AND ANALYSIS

Data Acquisition and Reduction

The spectra were obtained using an infrared heterodyne system (Betz *et al*. 1977) on one of the 1.65-m telescopes of the Infrared Spatial Interferometer (ISI; Hale *et al*. 2000) at Mount Wilson, California. The infrared heterodyne technique and its application to planetary atmospheres are described by Kostiuk (1994) and Kostiuk *et al*. (1997) in application to planetary atmospheres. Isolated emission lines of NH_3 near 10.7 μm were measured at a spectral resolution of $\sim$3.2 MHz ($\Delta\nu_\lambda = 10^{-4}$ cm^{-1}, $\nu_\lambda/\Delta\nu_\lambda \sim 10^7$). Integration times varied from 8 to 40 min over the observing period. The three lines of NH_3 that were measured and their molecular parameters (frequency, intensity, and lower state energy at 296 K) are summarized in Table I. The observations were made by actively tracking on an impact region. In the weeks following the impacts, tracking errors were large due to the lack of clear features to track on. This error can

TABLE II
Observation Summary

Impact region	UT Date 1994	Days after impact	aQ(2,2)	aQ(6,6)	aQ(9,8)
G	Jul 19	1	✓	✓	
G	Jul 22	4	✓	✓	✓
G	Aug 5	18	✓		
K	Jul 23	4	✓		
K	Jul 26	7	✓	✓	

be determined from individual scans and is taken into account in the analysis. Different transitions of NH_3 were measured at multiple impact sites on a given day. This work focuses on spectra obtained at the G and K impact regions following the impacts (Table II). Absolute spectral radiances were obtained using a lunar calibration, with conservative uncertainties of ∼10%.

General Analysis

In our analysis, the measured 3.2-MHz resolution was degraded to ∼8-MHz resolution (0.0003 cm^{-1}), more than adequate for resolving emission lineshapes of ∼200 MHz full width at half maximum (FWHM). The effective field-of-view (FOV) for analysis, including instrumental beam size and atmospheric seeing, is 2 arcsec diameter, ∼8000 km projected onto Jupiter. The plume splashback region for the G and K impacts is ≥10,000 km (Hammel *et al*. 1995, Jessup *et al*. 2000, Bézard *et al*. 1997), filling the FOV. Spectra were analyzed by comparison with models of the emergent molecular lines produced by our radiative transfer software package, BEAMINT (Hewagama *et al*., in preparation). The beam-integration technique involves dividing the beam aperture into multiple sections and producing a model spectrum for specified physical conditions such as temperature, abundance, planetary rotation, and mean viewing angle within each section of the beam. The broadening due to planetary rotation (∼150 MHz) is modeled by the software. The beam elements are combined, with beam element area and beam response weighting, to produce a beam-integrated spectrum. Since a single beam covers a relatively broad range of viewing angles on Jupiter, BEAMINT provides a more accurate characterization of an observed spectrum than a single-point mean viewing angle spectral model. This proved to be especially useful in the case of a spectrum with a large but known tracking error. We were able to recreate the larger broadening due to planetary rotation across a wider beam profile through the use of multiple multielement beams.

The radiative transfer portion of the program accepts molecular line parameters (Table I), arbitrary temperature and molecular mole fraction profiles, and planetary parameters. The radiative transfer calculation scales the molecular line intensities to the kinetic temperature corresponding to the region of line formation. The hydrogen broadened half width at half maximum (HWHM) for NH_3 used is 0.115 $cm^{-1}\,atm^{-1}$ at 200 K (Margolis and Poynter 1991), and the pressure-broadening temperature dependence is $T^{-0.5}$.

In our analysis, we investigated the variation of the beam-integrated spectrum, which results from changing the abundance and temperature distribution. Generally, the change in the spectrum is nonlinear; therefore we used a modified Levenberg–Marquardt algorithm to perform the least-squares fit of the model spectrum to the observations. Specifically, we used constant-with-height NH_3 mole fraction distributions over various altitude ranges (e.g., 150 to 1 mbar, 1-mbar level and higher). The range in the altitude of this constant-with-height distribution is selected as warranted by the lineshape. In most cases, the NH_3 mole fraction and temperature profile optimization were performed simultaneously using the Levenberg–Marquardt fitting technique. The errors are based on the *joint* probability distribution for the fit parameters and allow us to place conservative limits on the possible temperatures and amounts of NH_3 present in the stratosphere at different times following an impact. The quoted uncertainties give 68.3% confidence limits (i.e., 1σ) for a particular thermal profile and NH_3 mole fraction distribution.

Thermal Analysis

The initial thermal profile for the analysis is a quiescent jovian Voyager thermal profile roughly corresponding to the impact latitude (Fig. 3, profile *a*; Kostiuk *et al*. 1987). For each observing period, the profile was modified in the upper stratosphere in an attempt to fit our measurements on all emission lines

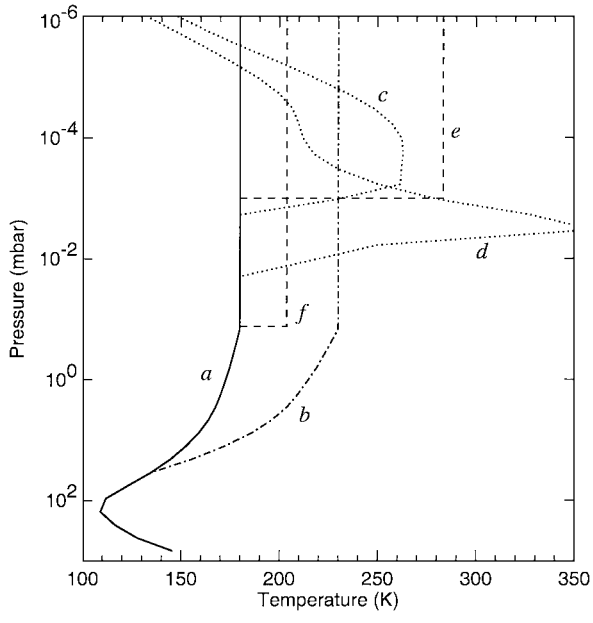

FIG. 3. Temperature profiles used for modeling. A quiescent Voyager profile (*a*) was used as a starting point. A uniform method of heating this profile (*b*) was found to be inadequate for the period soon after impact. Plume splashback temperature profiles (*c*, *d*) were used as guides to develop temperature profiles (*e*, *f*) that could simultaneously fit all NH_3 lines measured in the days following impact G.

simultaneously. Initial analyses uniformly modified (heated) the profile down to higher pressures (e.g., Fig. 3, profile *b*). This approach did not provide adequate fits to all measured lines for any attempted NH_3 altitude distribution.

Recently, a ballistic Monte Carlo and radiative–hydrodynamic treatment of the splashback process has been able to account for many SL9 phenomena, including several previously unexplained aspects (Harrington and Deming 2001, Deming and Harrington 2001 (hereafter HD–DH)). The splashback shocks for large impacts like G and K heat the atmosphere above approximately 0.01 mbar. Examples of residual heating from the HD–DH model are shown in Fig. 3, profiles *c* and *d*. Differences in the modeled profiles result from radial variations in the plume column density and from waves and turbulence following the splashback.

We used the HD–DH result of high-altitude heating due to the plume splashback as a guide for our thermal analysis. We modified the quiescent Voyager thermal profile above the 0.01-mbar level as well as above other high altitude levels, as opposed to our earlier uniform heating of the profile down to lower stratospheric altitudes. There was a great improvement in the ability to simultaneously model all line profiles from a particular observing day. The heating altitude, the temperature, and the NH_3 abundance and altitude distribution were simultaneously iterated until a best fit to all line profiles was achieved.

G Impact Region

G impact plus 1 day. The aQ(2,2) and aQ(6,6) NH_3 emission lines (Table I) were acquired from the G impact region 22 h after impact (Fig. 4). The two molecular lines were modeled simultaneously, using constant-with-height NH_3 mole fraction distributions with various lower altitude cutoffs, from 150 mbar (tropopause) to 0.3 mbar. As previously mentioned, thermal profiles based on uniform heating of a quiescent Voyager temperature profile above 35 mbar (e.g., Fig. 3, profile *b*) did not yield adequate fits to both lines simultaneously. Because the HD–DH plume splashback model indicated high-altitude heating, we tried heating the thermal profile above various high altitude levels. This resulted in adequate simultaneous fits to both lines.

Ranges in both NH_3 distribution cutoff altitudes and altitudes for heating the thermal profile were tested. Results indicate that NH_3 was primarily observed at altitudes above ~3 mbar. The best fit to the spectra places the observed NH_3 above the 1-mbar level (solid-line fit in Fig. 4). The resulting NH_3 mole fraction above the 1-mbar level was $(6.8 \pm 1.4) \times 10^{-6}$, and the column density was $(7.7 \pm 1.6) \times 10^{17}$ cm^{-2}. The best temperature profile was found by heating the quiescent profile above 0.001 mbar to 283 ± 13 K. The calibrated measured line brightness temperatures (>190 K) require significant heating at high altitudes where the line peaks are formed. The lineshapes also require contributions around the 1-mbar level to properly model the line wings. The heating can acceptably extend as low as the 0.003-mbar level, resulting in a comparable column density but requiring a lower temperature (240 K). The NH_3 can extend as low as the 3-mbar level with a poorer model fit to the line peaks, but it would allow a temperature of 255 K down to the 0.01-mbar level and result in about half the column density of the best-fit model. Extending the heating below ~0.01 mbar causes the peak of the aQ(2,2) model line to approach the intensity of the aQ(6,6) line, which is not seen in the data (Fig. 4,

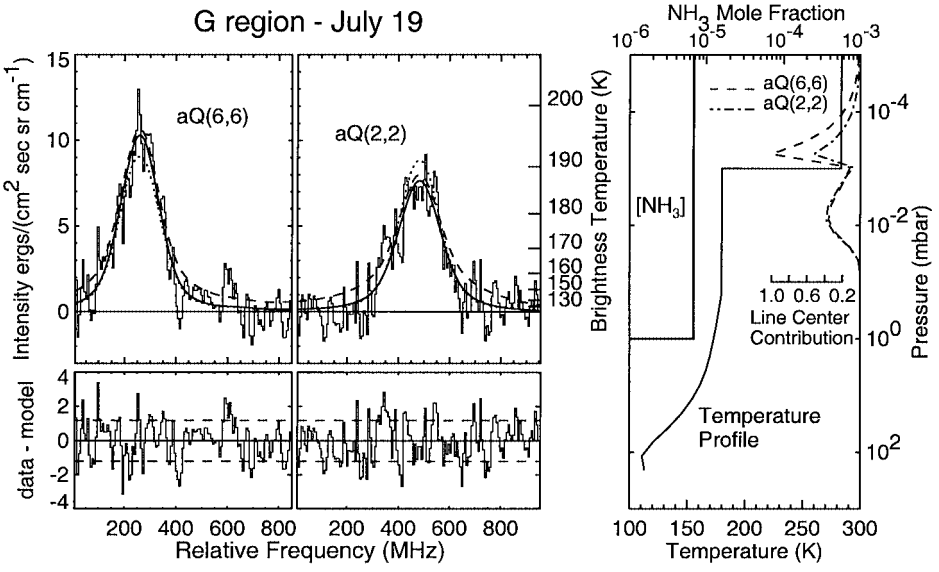

FIG. 4. G impact region spectra from July 19, 1994 (22 h after G impact). The model fit retrieved an NH_3 mole fraction of $(6.8 \pm 1.4) \times 10^{-6}$ above the 1-mbar level (column density $(7.7 \pm 1.6) \times 10^{17}$ cm^{-2}) and an increase in temperature above quiescence to 283 ± 13 K above the 10^{-3}-mbar level. The dashed model indicates the inclusion below the 1-mbar level of the retrieved NH_3 mole fraction found 18 days after impact (1.3×10^{-7}) and is not an acceptable model. The dotted model illustrates how the fit to the line peaks degrades when the heating of the thermal profile extends below the 0.01-mbar level (NH_3 mole fraction of 6.0×10^{-6} down to 1 mbar, with heating above 0.03 mbar to 201 K).

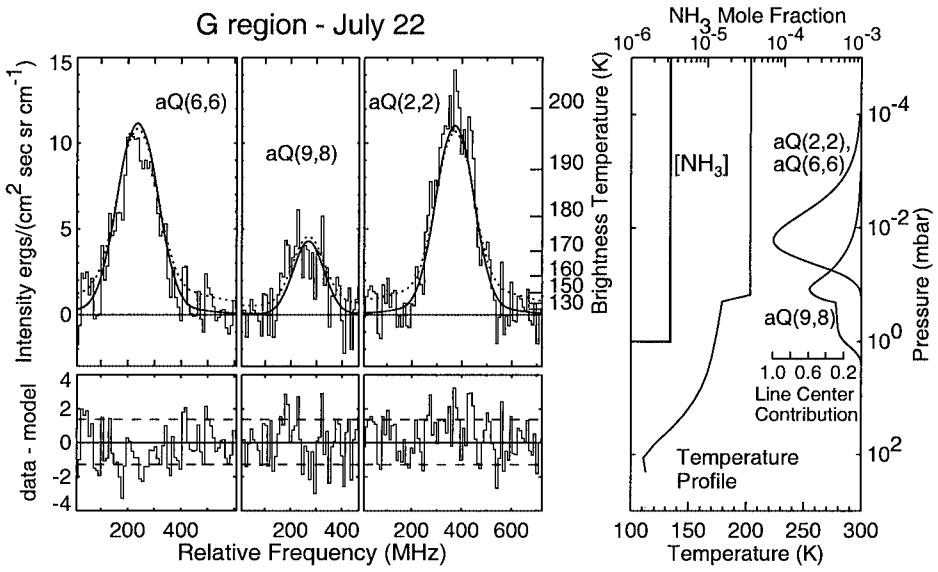

FIG. 5. G impact region spectra from July 22, 1994 (4 days after G impact). The best simultaneous fit to all three lines required an NH_3 mole fraction of $(3.2 \pm 0.7) \times 10^{-6}$ above 1 mbar (column density $(3.7 \pm 0.8) \times 10^{17}$ cm^{-2}) and the quiescent temperature profile heated to 204 ± 1 K above 0.2 mbar. The relative line center contribution functions illustrate the advantage of using lines of different lower state energies to probe different regions of the atmosphere. The contribution from the aQ(9,8) line comes from an altitude region lower than that of the aQ(2,2) and aQ(6,6) lines, which helps to limit the range of possible temperature and NH_3 mole fraction combinations that fit all three lines simultaneously. The dotted model illustrates how the wing fits degrade when NH_3 is included below the 3-mbar level (NH_3 mole fraction of 3.7×10^{-6} down to 10 mbar, with heating above 1 mbar to 205 K).

dotted model). Including NH_3 at altitudes lower than ~3 mbar results in excess wing contribution.

G impact plus 4 days. This was the one occasion on which all three different NH_3 emission lines, aQ(2,2), aQ(6,6), and aQ(9,8) (Table I), were observed on the same day within the G impact region. The aQ(2,2) and aQ(6,6) lines are strong lines of relatively low lower-state energies. The aQ(9,8) line is a weaker line of higher lower-state energy that probes deeper in the atmosphere, and its higher temperature sensitivity provides a tighter constraint on the thermal structure.

Our initial models that involved heating the atmosphere down to a higher pressure (e.g., Fig. 3, profile *b*) were able to fit the line shape of the stronger aQ(2,2) and aQ(6,6) lines but did not fit the aQ(9,8) line. When the model quiescent temperature profile was heated above higher altitudes, all three NH_3 emission lines could be fit simultaneously (Fig. 5). The requirement that all three lines be modeled simultaneously places limits on the possible thermal and NH_3 distributions that provide acceptable models. Measured line peak brightness temperatures again require significant heating at high altitudes (~0.1-mbar level). The aQ(9,8) line probes lower and constrains the abundance and temperature in its emitting region (Fig. 5, contribution functions). It was found that an NH_3 distribution only at altitudes above the 1-mbar level provided the best fit, with a mole fraction of $(3.2 \pm 0.7) \times 10^{-6}$ and a column density of $(3.7 \pm 0.8) \times 10^{17}$ cm^{-2}. The retrieved temperature profile was cooler (204 ± 1 K) than that found from the 1-day spectra, but the heating extended down to higher pressure (0.2 mbar). Heating had to extend at least down to the 0.03-mbar level, with the best fit extending down to 0.2 mbar. Thermal gradients and turbulence may account for this deeper but less pronounced heating than was modeled on the first day after impact. Distributions that included significant NH_3 at altitudes down to and below the 3-mbar level resulted in poor fits to the line wings (e.g., Fig. 5, dotted model), and models limiting NH_3 to altitudes above the 0.3-mbar level did not fit the aQ(9,8) peak well. Some of these models were still within 1σ of the best fit shown in Fig. 5, but the retrieved column densities for all of the acceptable models varied only by a factor of 2, and the temperatures of the heated region varied by only a few degrees.

G impact plus 18 days. The strong aQ(2,2) line was the only one measured on this day, but its mere presence indicates that NH_3 was still present in the stratosphere $2\frac{1}{2}$ weeks after impact G. As shown in Fig. 6, the line is quite broad. At 18 days postimpact, it was difficult to discern features to track on, and a tracking error of $\pm 7^\circ$ longitude (± 1.5 arcsec) was determined from the individual scans that compose this spectrum. This was taken into account by approximating the same tracking error, and ultimately the elongated beam shape, through the use of multiple beam positions in generating the model spectrum. This case in particular benefited from the beam-integration technique, as a mean viewing angle model did not fully take into account the range of rotational velocities across the elongated beam and resulted in a narrower line shape. Even with the tracking error taken into account, there is still additional broadening that can be accounted for by broadening due to higher pressure in the region probed (>1 mbar). The brightness temperature requires the temperature in the region of line formation to be at least 170 K.

The data were fit by uniformly varying the standard temperature profile. The best fits were within a few degrees of the

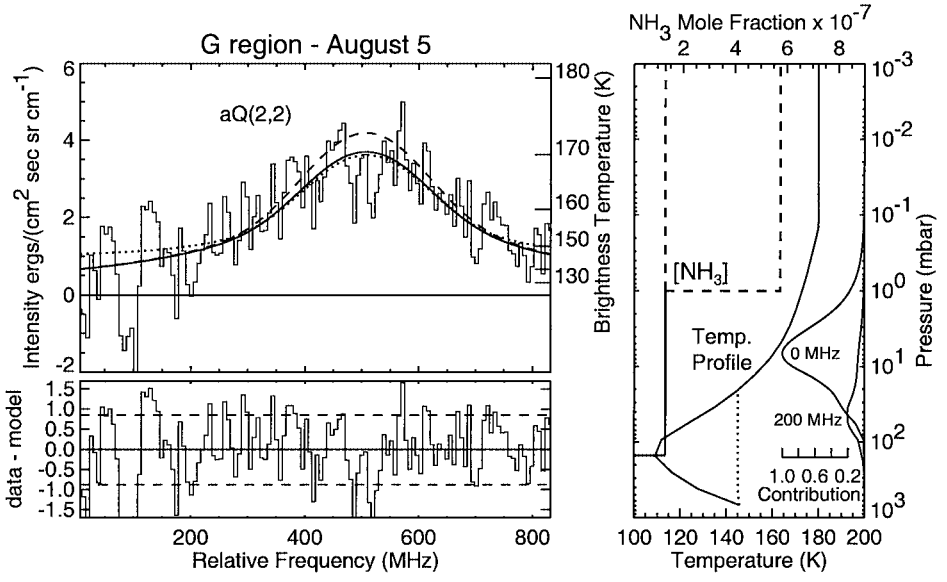

FIG. 6. G impact region spectrum from August 5, 1994 (18 days after G impact). The broad shape of this line indicates that the NH_3 contribution is mainly from the lower stratosphere, even when tracking errors are taken into account. For a quiescent temperature profile and an NH_3 distribution down to the tropopause, we retrieve a mole fraction of $(1.3 \pm 0.7) \times 10^{-7}$ (column density above 50 mbar $(7.3 \pm 1.7) \times 10^{17}$ cm^{-2}). The dotted model shows the maximum amount of tropopause heating that can be tolerated by the data, and the resulting NH_3 mole fraction is 1.1×10^{-7}. The dashed model includes the derived upper limit for NH_3 above the 1-mbar level of 6.5×10^{16} cm^{-2}.

quiescent profile, so a quiescent profile was adopted for the final NH_3 retrievals. A simple gray atmosphere radiative flux calculation (Deming and Harrington 2001) using the starting temperature suggested by the 4-day G observation indicates that a return to a quiescent upper stratospheric temperature by 18 days postimpact is reasonable. This is also consistent with results of Kostiuk *et al*. (1996), who indicated a return to near quiescent temperature ~8 days after the Q1 and R impacts, and with our results on the K region 7 days after impact (see below).

This spectrum acquired 18 days after impact cannot be modeled adequately using NH_3 distributed only above the 1-mbar level, as with spectra from the first days after impact. The spectrum can best be modeled using NH_3 distributed down to the tropopause (150 mbar). This distribution requires an NH_3 mole

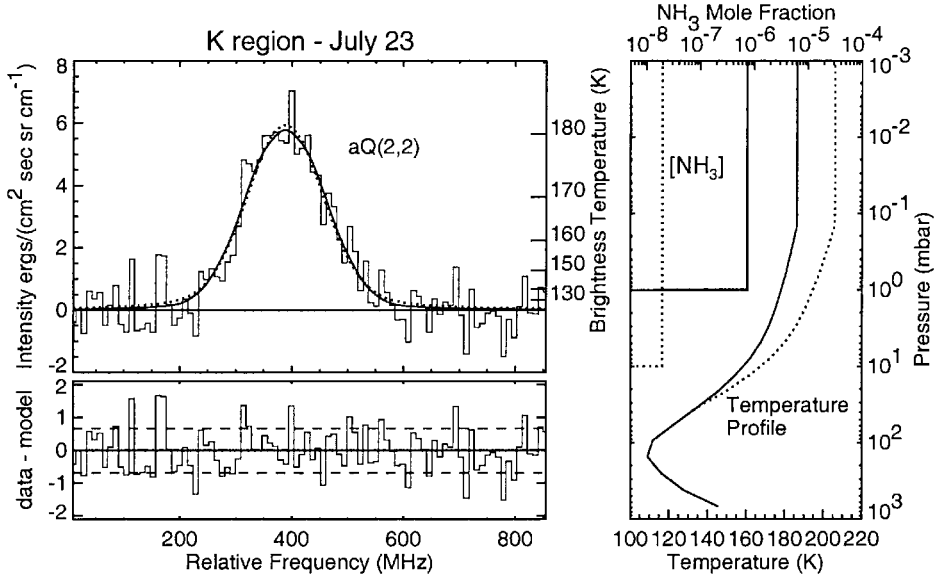

FIG. 7. K impact region spectrum from July 23, 1994 (4 days after K impact). Although more difficult to determine precisely, the temperature must be at least 187 K above 0.1 mbar, which results in an NH_3 mole fraction of $\sim 10^{-6}$ above 1 mbar ($\sim 10^{17}$ cm^{-2}). The dotted model illustrates that a higher temperature with a corresponding difference in NH_3 distribution can also provide an acceptable fit.

fraction of $(1.3 \pm 0.3) \times 10^{-7}$ (Fig. 6). The bulk of the line center contribution is from between ~2 and ~20 mbar (Fig. 6). The half-maximum line wing contribution (200 MHz from line center) is from ~50 mbar. The contribution below the ~50-mbar level is not as significant. The column density above the 50-mbar level for the retrieved mole fraction is $(7.3 \pm 1.7) \times 10^{17}$ cm^{-2}. This is as high as the NH_3 column densities retrieved closer to the impact time above the 1-mbar level, suggesting an additional lower altitude source for the NH_3. We derived an upper limit to the NH_3 abundance above the 1-mbar level by varying the mole fraction distribution as shown in Fig. 6 (dashed model). An upper limit to the NH_3 column density above the 1-mbar level of 6.5×10^{16} cm^{-2} was retrieved.

K Impact Region

K impact plus 4 days. Only the aQ(2,2) NH_3 line was measured at the K region 4 days after the K impact. Without additional lines, simultaneous NH_3 abundance and temperature retrieval is less constrained. However, fits to the line did indicate that the contribution comes primarily from above the few-mbar level, and the temperature is above quiescence. The better fits to this spectrum put an NH_3 mole fraction of $\sim 1.0 \times 10^{-6}$ at altitudes above 1 mbar, and a temperature in that region of 187 K (Fig. 7). The column density retrieved for this case is $(1.2 \pm 1.0) \times 10^{17}$ cm^{-2}. The 187 K temperature represents a lower limit. As indicated in Fig. 7, other combinations of temperature and NH_3 mole fraction (dotted curves) could provide acceptable fits to the single NH_3 line. The column density varied by no more than a factor of 2 for all the assumed profiles.

K impact plus 7 days. The aQ(2,2) and aQ(6,6) lines were both observed at the K impact region 1 week following the K impact. The retrieved temperature profiles were all within ±5 K of quiescent values. This is consistent with other retrievals (e.g., Kostiuk *et al.* 1996) for a comparable period after impact, and with radiative cooling calculations (Deming and Harrington 2001). The fit to a quiescent temperature profile (Fig. 3, profile *a*) is shown in Fig. 8. The lineshapes put the NH_3 at altitudes above 10 mbar, with a mole fraction of $(8.2 \pm 1.0) \times 10^{-8}$ and a column density of $(9.3 \pm 1.1) \times 10^{16}$ cm^{-2}.

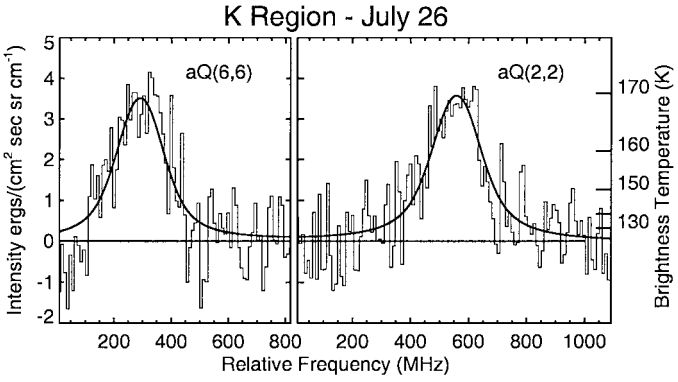

FIG. 8. K impact region spectrum from July 26, 1994 (7 days after K impact). These spectra can be fit using a quiescent profile, resulting in an NH_3 mole fraction of $(8.2 \pm 1.0) \times 10^{-8}$ above 10 mbar (column density $(9.3 \pm 1.1) \times 10^{16}$ cm^{-2}).

DISCUSSION

A summary of our retrievals for the G and K impact regions can be found in Table III. These retrieved results provide insight into the processes that occurred over the 18-day period following the SL9 fragment impacts. The spectral lineshapes measured provided information on the changes in the stratospheric thermal structure and the deposited NH_3 abundance and altitude distribution. This information can be used to test photochemical models of NH_3 in the jovian stratosphere, their temporal behavior, and dependence on temperature.

Thermal Behavior

We found that for the G impact region during the first few days after the G impact, the spectra required high-altitude heating, which is consistent with the HD–DH plume splashback model. High-altitude heating has also been suggested by other

TABLE III
Retrieval Results Summary[a]

Impact region	UT date 1994	Temperature	NH_3 mole fraction	Column density (cm^{-2})
G + 1 day	Jul 19	283 ± 13 K above 10^{-3} mbar	$(6.8 \pm 1.4) \times 10^{-6}$ above 1 mbar	$(7.7 \pm 1.6) \times 10^{17}$
G + 4 days	Jul 22	204 ± 1 K above 0.2 mbar	$(3.2 \pm 0.7) \times 10^{-6}$ above 1 mbar	$(3.7 \pm 0.8) \times 10^{17}$
G + 18 days	Aug 5	Quiescent (180 K)	$(1.3 \pm 0.3) \times 10^{-7}$ above 50 mbar	$(7.3 \pm 1.7) \times 10^{17}$
K + 4 days	Jul 23	~187 K above 0.1 mbar	$\sim 1.0 \times 10^{-6}$ above 1 mbar	$\sim 1.2 \times 10^{17}$
K + 7 days	Jul 26	Quiescent (180 K)	$(8.2 \pm 1.0) \times 10^{-8}$ above 10 mbar	$(9.3 \pm 1.1) \times 10^{16}$

[a] Uncertainties are precision of fits for the given model. See text for details.

observations (e.g., Bézard *et al*. 1997). The retrieved temperature was 283 K above the 0.001-mbar altitude level 1 day after impact. By 4 days after impact, the retrieved temperature had cooled to 204 K, but the heated region extended down to a few tenths of a mbar by this time.

The retrieved temperature changed by ~80 K over 3 days. That change was much larger than what would be expected from a simple gray atmosphere radiative cooling model that only included jovian material (Deming and Harrington 2001). However, if foreign opacity (e.g., cometary water) is introduced into their cooling model, the additional opacity increases the cooling rate. In the case of water opacity, in order to reproduce the drop in temperature that was retrieved from the data, <0.5% of the material was required to be water during that 3-day period. Thermal emission from small silicate particles has also been found to be an efficient mechanism for cooling the atmosphere (Bézard 1997). Dynamical mixing with cool jovian air may also have contributed to the observed temperature decrease.

The retrievals from the K region 4 days after impact, although not as precise, are also consistent with a heated stratosphere, with temperatures greater than 187 K. By 1 week after the K impact, the temperature appeared to have returned to a quiescent state. This is consistent with results on other impact regions (e.g., Kostiuk *et al*. 1996) after 1 week. We also see that by 18 days after the G impact, the upper stratospheric region appears to have returned to a quiescent temperature.

Ammonia Abundance

The NH_3 abundance retrievals for the 1- and 4-day post-G impact spectra indicate that the bulk of the observed NH_3 contribution originated from altitudes above 1 mbar. The retrieved column densities (Table III) are consistent with other IR measurements for G and other large impacts such as those of Orton *et al*. (1995), Kostiuk *et al*. (1996), and Conrath (personal communication, 1995) from SpectroCam-10 observations (Nicholson *et al*. 1994). HST UV observations (Noll *et al*. 1995, Atreya *et al*. 1995) retrieved lower NH_3 column densities, but their results and altitude distributions vary (Yelle and McGrath 1996) depending on the assumed altitude of the scattering layers. The discrepancy between UV and IR results may be due to the fact that the UV measurements concentrate on the central impact region, whereas this work is sensitive to the entire debris field from the reentered plume.

We found that by 18 days after the G impact, the spectrum could be fit using a quiescent temperature profile and an NH_3 distribution in the lower stratosphere. The retrieved column density is as high as those retrieved near the impact time above the 1-mbar level (Table III). The presence of this amount of NH_3 at these low altitudes suggests an additional source in the lower stratosphere. Griffith *et al*. (1997) suggested an additional thin-layer NH_3 source in the 15- to 30-mbar region ($1–3 \times 10^{17}$ cm^{-2}) for the K site ~11 days after impact for a quiescent thermal profile. For the G region, our lineshape does not require a thin-layer source. When we limited an NH_3 distribution to the 15- to 30-mbar region, significant heating (to ~170 K) in that region was required in order to obtain an adequate fit to our G impact spectrum, retrieving a column density of $\sim 7 \times 10^{16}$ cm^{-2}.

Analysis of the HST UV data by Yelle and McGrath (1996) suggests an NH_3 distribution below the 5-mbar level with a column density of 1.6×10^{18} cm^{-2} shortly after impact, comparable to our results at 18 days. We do not see evidence for this amount of NH_3 in the lower stratospheric region in the first few days following the impact, but the overwhelming contribution to our spectra from the upper stratosphere due to the plume splash-back heating may have masked the contribution from the much colder lower stratosphere. The 1- and 4-day spectra can statistically support (i.e., root mean square (RMS) within 1σ of best fit) an additional NH_3 mole fraction as high as 1.3×10^{-8} cm^{-2} below the 1-mbar level. Including our retrieved 18-day NH_3 mole fraction of 1.3×10^{-7} below the 1-mbar level in the 1-day model causes the line wings to fit quite poorly (Fig. 4, dashed model). Large amounts of NH_3 could be hidden from us soon after impact if it were present only below the 20-mbar level and if the region had not been heated significantly. It is also possible that we cannot probe below the few-mbar level early on due to the presence of dust or haze at the time of our observations. This is consistent with results by Kostiuk *et al*. (1996) 8.5 days after impact, which permit a haze layer up to the 10-mbar level. However, much lower spectral resolution measurements by Griffith *et al*. (1997) do probe down to the troposphere, where they observe an NH_3 absorption feature.

One possible source for the NH_3 in the lower stratosphere could be transport of NH_3 gas or ice crystals from the troposphere as a result of upward diffusion, dynamical mixing, and possible heating by the explosion of the impactor in or below the NH_3 ice cloud. For completeness, we determined that we could still model our spectrum with a maximum tropopause temperature of ~145 K (Fig. 6, dotted model). This is much warmer than the condensation temperature of a solar abundance of NH_3 for that pressure regime, which would permit the transport of NH_3 up to the lower stratosphere (Atreya *et al*. 1995). A tropopause temperature of 112 K is already above the condensation temperature for the NH_3 mole fraction that we measure (1.3×10^{-7}). A temperature of 112 K represents a 3-K increase in the tropopause temperature and is consistent with the maximum temperature increase allowed from measurements by Orton *et al*. (1995) and Bézard (1997) of the L impact region. Bézard (1997) finds that the increase may be due to stratospheric silicate emission, although our measurement of the NH_3 lineshapes would be unaffected by the silicate emission reported.

Ice crystal transport and subsequent sublimation mainly above the tropopause would be consistent with spectra obtained by Griffith *et al*. (1997) from the K impact, which show only a weak absorption underlying the NH_3 emission. Dynamical mixing due to increased temperatures in the upper troposphere could further enhance the NH_3 abundance in the lower stratosphere.

For the given best model atmospheres, the precision of the mole fraction retrievals was ~20% for each postimpact

observation (Table III). The accuracy of the retrievals is dependent on the accuracy of the atmospheric models, the line intensities, and the measured radiance calibration. The atmospheric models were tested as described in the individual sections corresponding to the different observations. The 10% uncertainty in calibration translates into a maximum uncertainty in mole fraction for the 1-, 4-, and 18-day G impact region measurements of 20, 5, and 40%, respectively.

The total mass of NH_3 within our FOV is determined to be at least 5×10^{12} g. The mass of a large cometary fragment is estimated to be $\sim 10^{14}$ g (Zahnle and Mac Low 1995, Lellouch *et al*. 1997). Nitrogen is believed to constitute ~2% of the cometary mass, and NH_3 <0.2% (cf. Mumma *et al*. 1994). We retrieved at least 2.5 times more NH_3 than can be supplied by nitrogen from a large cometary fragment, suggesting a primarily jovian source for the NH_3.

Photochemical Models

The NH_3 abundance retrievals can be used to test photochemical models. In the case of the G impact region, we observed NH_3 mainly above the 1-mbar level 1 day after impact. By 4 days, we saw a decrease in the abundance, and by 18 days the bulk of the NH_3 contribution was from below the 1-mbar level. This agrees qualitatively with photochemical models that predict preferential destruction of NH_3 at high altitudes. However, quantitatively we find that the decrease in the measured NH_3 column density is inconsistent with photochemical models, which predict a decrease slower than that observed.

Two simple one-dimensional photochemical models, which we describe here, were compared to our column densities retrieved from the observations spanning 18 days. The models have many elements in common. Both models step forward in time using a Runge–Kutta method, with a time step of one jovian day so that solar fluxes can be diurnally averaged. A solar zenith angle of 61°, applicable to the latitude of the SL9 impacts, was used in the calculations. The models compute the NH_3 photodissociation rate by assuming NH_3 is the only absorber in the wavelength range 160–221 nm. Opacity from other molecular absorbers (e.g., hydrocarbons, CS_2) and dust was neglected. Thus, the photodissociation rates, and hence NH_3 loss rates, are upper limits. The models also neglect the effects of mixing on the NH_3 distribution because the NH_3 photolysis lifetime is ~3 orders of magnitude shorter than the eddy mixing lifetime for a quiescent jovian lower stratosphere. It is shown below that this neglect of mixing, at least for the first ~20 days postimpact, is not correct. However, these chemistry-only models allow us to determine the maximum amount of NH_3 loss that could be attributed to photolysis and constrain the effects of dynamics on the NH_3 distribution.

The models differ in how the products of NH_3 photolysis were handled. In one, it was simply assumed that every time NH_3 is photolyzed, it is irreversibly lost to some other compound (maximum loss model). In the other model, a self-consistent chemistry scheme that allowed for some recycling of NH_3 (stand-alone model, Table IV) was used. This model also allowed the background atmosphere to cool with time to discern any temperature effects on the photochemical scheme. The model atmospheres used in the photochemical models were the same ones derived by the analysis of the NH_3 lines (Figs. 4, 5, and 7). The transitional temperature profiles were chosen by cooling the initial profiles over time according to a simple gray atmosphere cooling model (Deming and Harrington 2001).

Maximum loss model. The maximum loss model would fail to live up to its name only if there were another species that was chemically destroying NH_3, perhaps catalytically or powered by absorption of solar ultraviolet radiation at wavelengths longer than what NH_3 can absorb. To check this possibility, we compared the maximum loss model's predicted NH_3 column abundances over time to results of a more complex photochemical model that includes oxygen and sulfur chemistry given in Moses *et al*. (1995). The maximum loss model does indeed predict a more rapid loss with time than does the model of Moses *et al*. (1995). It is interesting to note that these two models predict a similar NH_3 loss from 0 to 9 days after impact. Thereafter, the model of Moses *et al*. (1995) predicts a much more gradual decline of NH_3 with time than does the maximum loss model. The maximum loss model represents an upper limit to the NH_3 loss, and it does not depend on temperature since there is no postphotolysis chemistry involved.

TABLE IV
NH_3 Photochemical System (Stand-Alone Model)

J1	$NH_3 + h\nu \rightarrow NH_2 + H$	[a] $\varphi = 1.0$, 160 nm $\leq \lambda \leq$ 221 nm	Wu *et al*. 1998
R1	$NH_3 + H \rightarrow NH_2 + H_2$	$k_1 = 9 \times 10^{-19} \times T^{2.4} \times e^{(-4990/T)}$	Ko *et al*. 1990
		[b] $k_{2,0} = 6 \times 10^{-30}$	Gordon *et al*. 1971
R2	$NH_2 + H + M \rightarrow NH_3 + M$	[b] $k_{2,\infty} = 2.66 \times 10^{-11}$	Pagsberg *et al*. 1979
R3	$H + H + M \rightarrow H_2 + M$	$k_3 = 2.7 \times 10^{-31} \times T^{-0.6}$	Baulch *et al*. 1992
		[b] $k_{4,0} = 1.3 \times 10^{-28}$	Mulenko 1987
R4	$NH_2 + NH_2 + M \rightarrow N_2H_4 + M$	[b] $k_{4,\infty} = 1.29 \times 10^{-11}$	Patrick and Golden 1984
R5	$NH_2 + H_2 \rightarrow NH_3 + H$	$k_5 = 2.09 \times 10^{-12} \times e^{(-4277/T)}$	Demissy and Lesclaux 1980

[a] φ is the quantum yield.
[b] For k_2 and k_4 the overall rate constant is given by $k_n = k_{n,0}k_{n,\infty}[M]/(k_{n,0}[M] + k_{n,\infty})$, where $[M]$ is the atmospheric number density.

Stand-alone model. The amount of NH_3 loss predicted by the stand-alone photochemical model depends on the atmospheric conditions. The reactions and rates for this model are given in Table IV. For pressures greater than 50 mbar, photolyzed NH_3 is recycled ~90% of the time. The remaining ~10% of the time, N_2H_4 (hydrazine) is formed. For pressures less than 50 mbar, the fraction of NH_3 recycled depends on the temperature of the model atmosphere. If the temperature is greater than 220 K (which our retrievals indicate 1 day after the G impact), then reaction R5 (Table IV) is an important reaction in the chemical scheme. Under these conditions, NH_3 is recycled ~99% of the time and is lost to N_2H_4 postphotolysis only ~1% of the time. Thus, this model predicted essentially no NH_3 loss via photolysis soon after impact (i.e., as long as the temperature was greater than 220 K). However, once the atmosphere cools below 220 K, recycling of NH_3 via R5 ceases in the model, and ~75% of the NH_3 is recycled while ~25% of it is lost to N_2H_4.

These results, however, are sensitive to the atomic hydrogen mixing ratio profile. While the models were being run and the results analyzed, it was noticed that the H mixing ratios from the stand-alone NH_3 photochemical model were greater than those from hydrocarbon photochemical models. In addition, the chemical lifetimes for H in the stand-alone model were longer than those in the hydrocarbon photochemical model over much of the region of interest. We then fixed the H mixing ratio profile to the values in the hydrocarbon photochemical model and ran the stand-alone model. For the cooler model atmospheres, the results were dramatic, with the stand-alone NH_3 photochemical model predicting the same NH_3 loss with time as the maximum NH_3 loss model. The lower H values essentially shut down R2 (Table IV), and the NH_3 was converted to N_2H_4 as fast as it could be photolyzed. However, for warm ($T \geq 220$ K) model atmospheres, recycling of NH_3 could still be carried out by R5, and NH_3 decay with time was intermediate to that of the maximum loss and the stand-alone NH_3 photochemical models with its own H mixing ratio profile.

Photochemical models and G impact retrievals. We compared the results of the maximum loss model to our NH_3 column density retrievals for the G impact. The maximum loss model gives an upper limit to the NH_3 loss. Since the first observation was at 1 day postimpact, the model was initialized with enough NH_3 above 1 mbar at time zero that the retrieved values (maximum, nominal, and minimum based on the retrieval and 1σ precision) were reproduced 1 day later. The model was then allowed to step forward in time to 4 days and the results (NH_3 column above 1 mbar) were compared to the retrieved values as shown in Fig. 9. In this optically thick situation, the NH_3 loss rate does not depend on the initial column density. What is readily apparent is that the NH_3 photochemical model, which is the maximum loss model, cannot explain the decrease in the observed NH_3 column. Over this 3-day period, the maximum photochemical loss model loses a total of 7×10^{16} NH_3 molecules cm^{-2}, which is a loss rate (flux) of -2.7×10^{11} NH_3 molecules cm^{-2} s^{-1}. In comparison, the retrievals from the observations require

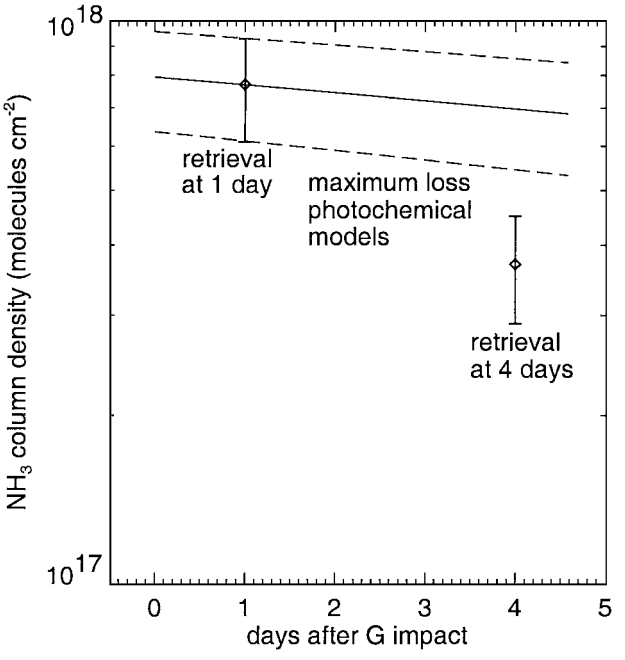

FIG. 9. Solid vertical bars represent the range in derived NH_3 column density above the 1-mbar level at 1 and 4 days after the G impact. The curves are the NH_3 column density above 1 mbar as a function of time calculated by the maximum NH_3 loss photochemical model. The initial NH_3 values in the photochemical models were set to reproduce the retrieved values at 1 day. The solid curve is the model based on the nominal 1-day retrieval, and the dashed curves are the models based on the upper and lower limits of the retrieval.

a total loss of $(4.0 \pm 2.4) \times 10^{17}$ NH_3 molecules cm^{-2}, or a loss rate (flux) of $-1.5^{+1.0}_{-0.9} \times 10^{12}$ NH_3 molecules cm^{-2} s^{-1}. At best, the maximum loss model, which gives an upper limit to the loss, can account for ~40% of the NH_3 loss required by the retrievals. Also, the stand-alone model, which is a more realistic model, loses NH_3 at an even slower rate. Clearly, during the first 4 days after the G impact, impact and atmospheric dynamics dominate over photochemistry. The derived value of K, the eddy diffusion coefficient, that supports a removal mechanism through downward flux (and condensation in lower, cooler regions) is greater than 10^7 cm^{-2} s^{-1}, i.e., is three orders of magnitude greater than the quiescent value. Ammonia would have to diffuse down half of a scale height over 3 days to remove enough from above the 1-mbar level, and we did not observe that. Therefore, downward diffusion of the NH_3 does not appear to be the dominant removal mechanism. The combined effect of spreading, mixing with NH_3-free jovian air, and photolysis may account for the observed decrease in our retrieved column density. Assuming that the drop in column density at altitudes above 1 mbar over the 3 days is due to uniform horizontal spreading alone, the inferred radial spreading velocities range from 3 to 12 m/s. This is consistent with spreading velocities obtained by Hammel *et al.* (1995), who retrieved velocities from 0 to 40 m/s from other impact regions using Hubble Space Telescope WFPC2 images. The velocities depend on the position relative to the site of impact and the altitude region probed (velocities decrease with altitude).

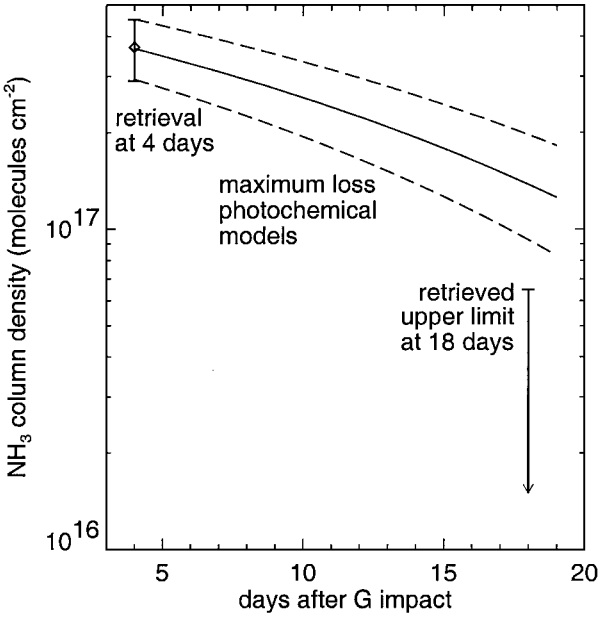

FIG. 10. Solid vertical line at 4 days represents the range in derived NH_3 column density above the 1-mbar level 4 days after the G impact. The derived upper limit at 18 days is shown. The curves are the NH_3 column density above 1 mbar as a function of time calculated by the maximum NH_3 loss photochemical model. The model was initialized with the observed range in NH_3 at 4 days postimpact and stepped forward in time 14 days. The solid curve is the model based on the nominal 4-day retrieval, and the dashed curves are the models based on the upper and lower limits of the retrieval.

Since the maximum loss NH_3 photochemical model failed to reproduce the 4-day postimpact retrievals when started at 0 days, we reinitialized the model before analyzing the time period between 4 and 18 days postimpact. The model was started with the observed 4-day postimpact NH_3 distribution and was allowed to step forward in time 14 days (to 18 days postimpact). A comparison of the photochemically derived NH_3 loss to our retrieved 18-day upper limit above the 1-mbar level of 6.5×10^{16} cm^{-2} is shown in Fig. 10. Once again, even the maximum loss model cannot reproduce the observed decrease in the NH_3 column. However, photochemical loss is becoming more important. Since this is no longer an optically thick situation, the NH_3 loss rate depends on the amount of NH_3 present. The model that is initialized with the lower limit column density of 2.9×10^{17} NH_3 molecules cm^{-2} loses 2.0×10^{17} NH_3 molecules cm^{-2} over the 14-day period, resulting in a loss rate (flux) of -1.6×10^{11} NH_3 molecules cm^{-2} s^{-1}. In comparison, the observations require a total loss of 2.2×10^{17} NH_3 molecules cm^{-2}, or a loss rate (flux) of -1.9×10^{11} NH_3 molecules cm^{-2} s^{-1} for this extreme case (minimum NH_3 loss supported by the observations). The maximum loss model can account for up to ~90% of the observed NH_3 loss. However, it should be noted again that any more realistic model that includes such things as recycling of NH_3 postphotolysis (e.g., the stand-alone model) or UV shielding of NH_3 by dust and other absorbers would only have a slower rate of NH_3 loss.

We find photochemistry to be too slow/inefficient to account for the retrieved decay of NH_3 column density above the 1-mbar level over the first 18 days postimpact. The opposite was concluded by Griffith *et al.* (1997) for the K impact region. They retrieved an NH_3 column density of $(0.5–2) \times 10^{16}$ cm^{-2} above the ~0.1-mbar level 21 h after impact, and the same results at 6 days postimpact with the decrease in NH_3 emission attributed to stratospheric cooling. At 11–12 days postimpact, they could place only upper limits of 10^{14} cm^{-2} above the 0.1-mbar level and 3×10^{15} cm^{-2} above the 5-mbar level. They compared these retrievals with the NH_3 photochemical loss rates of 3×10^{16} cm^{-2} over 3 days and 8×10^{16} cm^{-2} over 9 days from Moses *et al.* (1995). Griffith *et al.* (1997) concluded that the NH_3 must have been shielded from photolysis by either dust or another molecular absorber in the UV to explain the presence of NH_3 above the 1-mbar level 6 days postimpact. They found that the virtual disappearance of NH_3 from above the 5-mbar level by 11–12 days postimpact could be adequately explained by the Moses *et al.* (1995) loss rates. However, those loss rates were based on higher column densities, $\sim 10^{17}$ cm^{-2}. This is important because the NH_3 destruction rate due to photolysis is proportional to the amount of NH_3 present. Applying those loss rates to the Griffith *et al.* derived NH_3 column densities overestimates the NH_3 photolysis loss.

To investigate this further, we used our maximum loss rate model to analyze the K impact retrievals of Griffith *et al.* (Note that this model is consistent with Moses *et al.* (1995); i.e., it either reproduces or overestimates the Moses *et al.* NH_3 decay with time when started with the same initial NH_3 column density.) In all cases, we assumed that the initial NH_3 mole fraction was constant with height for all pressures less than 1 mbar. It is only if we initialize the model with the lower bound of NH_3 column density observed at 21 h postimpact, that we can produce an NH_3 column at 11–12 days lower than the Griffith *et al.* upper limits. Specifically, to allow the model-predicted NH_3 to be less than their upper limits for $p < 0.1$ mbar and $p < 5$ mbar at 11–12 days, the initial NH_3 column must be $\leq 6 \times 10^{14}$ cm^{-2} for $p \leq 0.1$ mbar and $\leq 2 \times 10^{16}$ cm^{-2} for $p \leq 5$ mbar. But this is the *maximum possible* photolytic loss, representing an upper limit to the loss. Shielding and postphotolysis recycling of NH_3 are not allowed in the model.

We propose instead the following possible interpretation of the K impact retrievals of Griffith *et al.* (1997). While the 21-h and 6-day postimpact retrievals do not *require* a decrease in the NH_3 column above 1 mbar, they do *allow* a decrease similar to the one seen in our G impact retrievals over 4 days (~50%), which we ascribe to dynamics. While the maximum NH_3 loss model can produce this permitted decline in the NH_3 column abundance, we do not consider it likely, because UV shielding by dust or another molecule and increased NH_3 recycling in the hot stratosphere via R5 likely caused the model to overestimate the NH_3 loss rate. Thus, over the first ~14 days postimpact, for both G and K impact sites, dynamical mixing with NH_3-free jovian air appears to dominate over

photochemical destruction in the observed decrease in the NH_3 column.

CONCLUSIONS

We found significant heating of the upper stratosphere in the days after the impacts as a result of the plume splashback (204–283 K). Return to a quiescent temperature takes place in about 1 week. The rate of cooling observed indicates that opacity equivalent to <0.5% water was present in the G region between 1 and 4 days postimpact.

In the first days after the G impact, the observed NH_3 appears to be primarily from plume material injected into the upper stratosphere at altitudes above 1 mbar. The retrieved NH_3 mass in our FOV is at least 25 times greater than what would be expected from a large cometary fragment. This points to a jovian source for the bulk of the NH_3 observed. The drop in NH_3 column density between 1 and 4 days postimpact (7.7×10^{17} to 3.7×10^{17} cm^{-2}) cannot be explained by photolysis alone. At most, photochemical destruction of NH_3 can account for ~40% of the observed decrease (maximum loss model). The region in the jovian stratosphere where NH_3 was present, and hence where NH_3 photolysis was occurring, was warm ($T > 220$ K) at the time. Under those conditions, NH_3 is efficiently recycled and the maximum loss model grossly overestimates the NH_3 photochemical loss rate. It is likely that a combination of mixing with NH_3-free jovian air, horizontal spreading of the plume material, and photolysis could account for the changes in NH_3 abundance.

Eighteen days after the G impact, we find a high total NH_3 column abundance of $(7.3 \pm 1.7) \times 10^{17}$ cm^{-2}, with the bulk of the NH_3 contribution coming from altitudes well below 1 mbar. The upper limit on NH_3 column density 18 days after impact above the 1-mbar level is 6.5×10^{16} cm^{-2}. This suggests a second source for NH_3 at the higher atmospheric pressures, possibly upwelling from Jupiter's troposphere around a heated and turbulent central impact region, which may have been initially masked by dust and haze. The time period between 4 and 18 days postimpact appears to be a period of transition in importance between horizontal spreading and the photochemical loss of NH_3. The maximum loss NH_3 photochemical model can account for up to ~90% of the observed NH_3 loss. This simple model may be more applicable by 18 days postimpact, as the jovian stratosphere has cooled down to the point where recycling of NH_3 after photolysis is less efficient. Also, if the atomic hydrogen number densities are lowered by reactions with other species, then NH_3 recycling becomes very inefficient. Even so, we are overestimating the importance of NH_3 photolytic loss, as the column density we used above the 1-mbar level is an upper limit.

The SL9 event provided a unique opportunity to study the photochemistry and residence time of NH_3 in the stratosphere of Jupiter, where it is not normally present. These results emphasize the importance of high-resolution infrared measurements of multiple spectral features over extended periods as probes of the temporal variability of stratospheric temperature and abundance distributions of NH_3 injected into the jovian stratosphere.

ACKNOWLEDGMENTS

The authors thank Drake Deming for informative discussions and suggestions. The University of Colorado authors thank Prof. C. H. Townes for the use of the Infrared Spatial Interferometer (ISI) facility on Mt. Wilson for these observations. This work was supported by the NASA Planetary Astronomy and Planetary Atmospheres Programs. Work at University of Colorado was supported by NASA Grant NAGW-3196, and the University of California ISI facility was supported by ONR Grant N00014-89-J-1583 and NSF Grants AST-9016474, AST-9119317, and AST-9321289.

REFERENCES

Atreya, S. K., S. G. Edgington, L. M. Trafton, J. J. Caldwell, K. S. Noll, and H. A. Weaver 1995. Abundances of ammonia and carbon disulfide in the jovian stratosphere following the impact of Comet Shoemaker–Levy 9. *Geophys. Res. Lett.* **22**, 1625–1628.

Baulch, D. L., C. J. Cobos, R. A. Cox, C. Esser, P. Frank, Th. Just, J. A. Kerr, M. J. Pilling, J. Troe, R. W. Walker, and J. Warnatz 1992. Evaluated kinetic data for combustion modelling. *J. Phys. Chem. Ref. Data* **21**, 411.

Betz, A. L., E. C. Sutton, and R. A. McLaren 1977. Infrared heterodyne spectroscopy in astronomy. In *Laser Spectroscopy III* (J. L. Hall and J. L. Carlsten, Eds.), Springer Series in Optical Sciences, Vol. 7, pp. 31–38. Springer-Verlag, Berlin/Heidelberg/New York.

Betz, A., R. Boreiko, M. Bester, W. C. Danchi, and D. Hale 1994. Stratospheric ammonia in Jupiter as a result of Comet SL-9. In *Abstracts for Special Sessions on Comet Shoemaker–Levy 9, The 26th Meeting of the Division for Planetary Sciences, Washington DC, 31 Oct.–4 Nov. 1994*, p. 25.

Bézard, B. 1997. Long-term response of Jupiter's thermal structure to the SL9 impacts. *Planet. Space Sci.* **45**, 1251–1270.

Bézard, B., C. A. Griffith, D. Kelly, J. Lacy, T. Greathouse, and G. Orton 1997. Thermal infrared imaging spectroscopy of Shoemaker–Levy 9 impact sites: Temperatures and HCN retrievals. *Icarus* **125**, 94–120.

Deming, D., and J. Harrington 2001. Models of the SL9 impacts. II. Radiative–hydrodynamic modeling of the plume splashback. *Astrophys. J.* **561**, 468–480.

Demissy, M., and R. Lesclaux 1980. Kinetics of hydrogen abstraction by NH_2 radicals from alkanes in the gas phase: A flash photolysis–laser resonance absorption study. *J. Am. Chem. Soc.* **102**, 2897.

Goldstein, J. J. 1989. Ph.D. thesis, University of Pennsylvania, Philadelphia.

Gordon, S., W. Mulac, and P. Nangia 1971. Pulse radiolysis of ammonia gas. II. Rate of disappearance of the $NH_2(X^2_{B1})$ radical. *J. Phys. Chem.* **75**, 2087.

Griffith, C. A., B. Bézard, T. K. Greathouse, D. M. Kelly, J. H. Lacy, and K. S. Noll 1997. Thermal infrared imaging spectroscopy of Shoemaker–Levy 9 impact sites: Spatial and vertical distributions of NH_3, C_2H_4, and 10-μm dust emission. *Icarus* **128**, 275–293.

Hale, D. D. S., M. Besler, W. C. Danchi, W. Fitelson, S. Hoss, E. A. Lipman, J. D. Monnier, P. G. Tuthill, and C. H. Townes 2000. The Berkeley Infrared Spatial Interferometer: A heterodyne stellar interferometer for the midinfrared. *Astrophys. J.* **537**, 998–1012.

Hammel, H. B., and 16 colleagues 1995. HST imaging of atmospheric phenomena created by the impact of Comet Shoemaker–Levy 9. *Science* **267**, 1288–1296.

Harrington, J., and D. Deming 2001. Models of the SL9 impacts. I. Ballistic Monte–Carlo plume. *Astrophys. J.* **561**, 455–467.

Jessup, K. L., J. T. Clarke, G. E. Ballester, and H. B. Hammel 2000. Ballistic reconstruction of HST observations of ejecta motion following Shoemaker–Levy 9 impacts into Jupiter. *Icarus* **146**, 19–42.

Ko, T., P. Marshall, and A. Fontijn 1990. Rate coefficients for the $H + NH_3$ reaction over a wide temperature range. *J. Phys. Chem.* **94**, 1401.

Kostiuk, T. 1994. Physics and chemistry of upper atmospheres of planets from infrared observations. *Infrared Phys. Technol.* **35**, 243–266.

Kostiuk, T., F. Espenak, M. J. Mumma, D. Deming, and D. Zipoy 1987. Variability of ethane on Jupiter. *Icarus* **72**, 394–410.

Kostiuk, T., D. Buhl, F. Espenak, P. Romani, G. Bjoraker, K. Fast, T. Livengood, and D. Zipoy 1996. Stratospheric ammonia on Jupiter after the SL9 collision. *Icarus* **121**, 431–441.

Kostiuk, T., K. Fast, T. A. Livengood, J. Goldstein, T. Hewagama, D. Buhl, F. Espenak, and K. H. Ro 1997. Ethane abundance on Titan. *Planet. Space Sci.* **45**, 931–939.

Lellouch, E., B. Bézard, R. Moreno, D. Bockelée-Morvan, P. Colom, J. Crovisier, M. Festou, D. Gautier, A. Marten, and G. Paubert 1997. Carbon monoxide in Jupiter after the impact of Comet Shoemaker–Levy 9. *Planet. Space Sci.* **45**, 1203–1212.

Margolis, J., and R. Poynter 1991. Low temperature hydrogen broadened linewidths of ammonia in the (0,1,0,0)–(0,0,0,0) band. *Appl. Opt.* **30**, 3023–3028.

Moses, J. I., M. Allen, and G. R. Gladstone 1995. Nitrogen and oxygen photochemistry following SL9. *Geophys. Res. Lett.* **22**, 1601–1604.

Mulenko, S. A. 1987. The application of an intracavity laser spectroscopy method for elementary processes study in gas-phase reactions. *Rev. Roum. Phys.* **32**, 173.

Mumma, M. J., P. R. Weissman, and S. A. Stern 1994. Comets and the origin of the Solar System: Reading the Rosetta Stone. In *Protostars and Planets III* (E. H. Levy and J. I. Lunine, Eds.), p. 1177. Univ. of Arizona Press, Tucson.

Nicholson, P., and 13 colleagues 1994. Principal results from Palomar observations of the Shoemaker–Levy 9 impacts. In *Abstracts for Special Sessions on Comet Shoemaker–Levy 9, The 26th Meeting of the Division for Planetary Sciences, Washington, DC, 31 Oct.–4 Nov. 1994*, p. 20.

Noll, K. S., M. A. McGrath, L. M. Trafton, S. K. Atreya, J. J. Caldwell, H. A. Weaver, R. V. Yelle, C. Barnet, and S. Edgington 1995. HST spectroscopic observations of Jupiter after the collision of Comet Shoemaker–Levy 9. *Science* **267**, 1307–1313.

Orton, G., and 57 colleagues 1995. Collision of Comet Shoemaker–Levy 9 with Jupiter observed by the NASA infrared Telescope Facility. *Science* **267**, 1277–1288.

Pagsberg, P. B., J. Eriksen, and H. C. Christensen 1979. Pulse radiolysis of gaseous ammonia–oxygen mixtures. *J. Phys. Chem.* **83**, 582.

Patrick, R., and D. M. Golden 1984. Kinetics of the reactions of NH_2 radicals with O_3 and O_2. *J. Phys. Chem.* **88**, 491.

Rothman, L. S., R. R. Gamache, R. H. Tipping, C. P. Rinsland, M. A. H. Smith, D. C. Benner, V. M. Devi, J.-M. Flaud, C. Camy-Peyret, A. Perrin, A. Goldman, S. T. Massie, L. R. Brown, and R. A. Toth 1992. The HITRAN molecular database: Editions of 1991 and 1992. *J. Quant. Spectrosc. Radiat. Transfer* **48**, 469–507.

Wu, C. Y. R., F. Z. Chen, D. L. Judge, and J. Caldwell 1998. Temperature-dependent photoabsorption study of atmospheric gases with application to planetary atmospheres. In *NASA Laboratory Space Science Workshop, Harvard–Smithsonian Center for Astrophysics, Conference Proceedings*, pp. 262–265.

Yelle, R. V., and M. A. McGrath 1996. Ultraviolet spectroscopy of the SL9 impact sites. I. The 175–230 nm region. *Icarus* **119**, 90–111.

Zahnle, K., and M.-M. Mac Low 1995. A simple model for the lightcurve generated by a Shoemaker–Levy 9 impact. *J. Geophys. Res. Lett.* **100**, 16,885–16,894.